Outmost Cationic Surface Charge of Layer-by-Layer Films Prevents Endothelial Cells Migration in Three-dimensional Tissues

*Jinfeng Zeng,[1] Sven Heilig,[2] Matthias Ryma,[2] Jürgen Groll[2] and Michiya Matsusaki[1,3]**

J. Zeng, M. Matsusaki

[1]Department of Applied Chemistry, Graduate School of Engineering, Osaka University, 2-1 Yamadaoka, Suita, Osaka 565-0871, Japan.

*Corresponding author, Email: m-matsus@chem.eng.osaka-u.ac.jp

S. Heilig, M. Ryma, J. Groll

[2]University of Würzburg, Pleicherwall 2, 97070 Würzburg, Germany.

M. Matsusaki

[3]Joint Research Laboratory (TOPPAN) for Advanced Cell Regulatory Chemistry, Osaka University, Suita, Osaka, Japan.

Keywords: positively-charged nanofilms, basement membrane, cell migration, ECs sprouts, patterned vascular tissue

Abstract:

Tissues and organs possess an organized cellular arrangement that enables their unique functions. However, conventional three-dimensional (3D) encapsulation techniques fail to recapitulate this complexity due to the cell migration during cell culture. In biological tissues, basement membranes (BMs) are essential to mechanically support cellular organization. In this study, we found that positively-charged outmost surface of multilayered nanofilms, fabricated through LbL assembly of poly-L-lysine (PLL) and dextran (Dex) via hydrogen bonds, stimulated the barrier functions of BMs. This type of artificial BMs (A-BMs) demonstrate enhanced barrier properties in comparison to other type ofA-BMs composed of BM component such as collagen type IV and laminin. Such an enhancement is potentially associated with the outmost positive layer, which inhibits the sprouting of endothelial cells (ECs) and effectively prevents EC migration over a 14-day period, aligning with the regeneration timeline of natural BMs in 3D tissues. In the

end, 3D organized vascular channels are successfully engineered through the sequential processes of spreading smooth muscle cells (SMCs), *in-situ* assembly of PLL/Dex nanofilms and endothelialization of ECs, which would provide a reliable platform for evaluating the efficacy of drugs, investigating nanotoxicology, and advancing the development of regenerative medicine.

1. Introduction

Numerous mammalian tissues possess distinct cellular configurations, characterized by structural patterning and compositional heterogeneity, thereby enabling their unique functions within biological systems.[1] However, conventional tissue engineering techniques usually fail to recapitulate this complexity due to the random encapsulation of multiple types of cells, including both bottom-up[2–4] and top-down[5,6] methods. Therefore, to accurately mimic the functionality of living systems, it is essential to develop innovative strategies that ensure reproducibility in recreating the complexity of structures and scalability for widespread application.

Since 1994, there has been notable recognition and endeavor towards the fabrication of patterns. Ingber *et al.* designed, for the first time, the patterned two-dimensional (2D) substrate by soft-lithographic technique to position cells in predetermined locations.[7] Since then, advanced methodologies, such as dip-pen nanolithography,[8] nanoimprint lithography,[9] and molecular assembly patterning,[10] have been developed for depositing biomolecules individually on 2D substrates, facilitating the evaluation of cell behaviors in patterned co-culture systems. Nevertheless, these methodologies for engineering substrate surfaces with selective adhesiveness are not suitable for fabricating similar patterns within complex 3D constructs. Primo and Mata reviewed the recent techniques for creating 3D patterns of functional molecules within hydrogels.[1] Most of these approaches, including 3D photo-patterning, advanced microfluidics, electric and magnetic fields, as well as precise chemical design, concentrated on producing functional biological scaffolds. However, they have not addressed the challenges of selectively encapsulating multiple types of cells in three dimensions. Ma[11] and Onoe[12] reported successively the fabrication of compartmentalized hydrogel microparticles for efficient 3D cell culture. Recently, Hu and his group[13] also reported Janus alginate/poly-L-lysine/alginate (APA) microcapsules, which facilitate the spatial organization of multi-

cellular co-cultures through a programmable electrodeposition method. Despite these advances, these approaches still suffer from the lack of substantial barriers to maintain their organized tissue structures. Precise cell locations were easily destroyed because of the cell migration during the cell culture period, such as the endothelial cells (ECs) sprouting toward other tissues.[14,15] Furthermore, macroscopically, encapsulated cells were still in a random state, limiting the construction of anatomic-scale organized tissue models. Until now, only the work in Takayama group[16] succeeded at seeding different types of cells on existing cell monolayer based on an optimized polymeric aqueous biphasic system (ATPS) of polyethylene glycol and dextran solution. However, cell behaviors in high concentration ATPS solution and the stability to keep cell compartmentalization are still unclear.

Inspired by the hierarchical structures of native tissues/organs, where basement membrane (BM) acts as a support platform to regulate cellular behaviors and adjust the passage of both cells and large molecules.[17–20] The successful construction of artificial BMs (A-BMs) *in vitro* might significantly contribute to the fabrication of 3D organized tissue structures. BM has been identified as a dense, continuous sheet-like structure with nanometer-scale thickness.[21,22] Different strategies were developed to duplicate the structure and function of BMs from simple polymer membranes[23,24] to electrospun scaffolds.[25–28] The electrospun nanofiber meshes permitted bipolar cultivation of epithelial (endothelial) cells and mesenchymal cells, forming human primary alveolar-capillary barrier models[25,28] and skin models[29]. However, the *in-situ* preparation of A-BMs with nanometer-scale thickness on existing cell layers is challenging due to the utilization of specific apparatus, the complexity of the process, and the application of organic solvents. Considering the diversities in structure and shape of tissues among different body parts, such as the tubular configuration in blood vessels, and the irregular lamellar architecture in the liver and intestinal wall, there is a compelling need for advanced methodologies to *in-situ* fabricate adaptable A-BMs tailored to the variable and intricate architectures within 3D tissues.

For an ultra-thin nanofilm construction, the layer-by-layer (LbL) assembly technique offers a robust and versatile method for controllable bio-coating at a micro-/nano-meter scale. The assembly of multilayered films was achieved by immersing the substrate into

different solutions for the alternate deposition,[30,31] thereby contributing to the advantage of LbL assembly in preparing ultra-thin films with customized shapes and controllable thickness. In our group, a multifunctional A-BM was fabricated by the assembly of collagen type IV (Col-IV) and laminin (LM) which are derived from the main components of BMs.[32,33] Assembled Col-IV/LM nanofilms exhibited controllable thickness and size-controllable molecular permeability. They facilitated cell adhesion and differentiation and enabled effective heterogeneous cellular communication through the porous fiber networks. Moreover, with the assistance of A-BMs, patterned cell co-culture could be maintained for up to 5 days. Without them, ECs migrated and sprouted into fibroblast layers, forming random capillaries. This suggests the significance of adaptable A-BMs in preserving the integrity of compartmentalized cell co-culture systems. However, the literature reveals that a partly plugged mesh of BM proteins deposited by the immortalized alveolar type II epithelial cells cultured with Matrigel *in vitro* for 5 days and the formation of a thin BM sheet took around 10 days.[34] The barrier effect of A-BMs, therefore, should be further enhanced to keep long-term cell compartmentalization until the re-construction of natural BMs in 3D tissues.

In contrast to the unchangeable conformation of proteins, polyelectrolyte assembled films generally have homogeneous charge distribution, adaptable conformation, and are more stable co-cultured with cells. Moreover, it has been reported that directional ECs sprouts tend to form towards the negatively charged membrane surface of apoptotic cells and sprouting ECs typically migrate towards the cathode in a direct current electric field.[35–37] This suggests that a polyelectrolyte nanofilm with a positively charged outermost layer could effectively prevent the migration of ECs. For proof-of-concept, we construct a positively charged nanofilm via hydrogen bonds between poly-L-lysine (PLL) and dextran (Dex) to mimic the barrier effect of BMs to prevent EC migration. In this study, we evaluate the microstructure of PLL/Dex nanofilms (NFs) and conduct a comparative analysis of cell adhesion propoties and barrier functions of PLL/Dex NFs in comparison to Col-IV/LM NFs reported previously and a series of polyelectrolyte films (Scheme 1). A significant enhancement in the barrier properties of the newly prepared A-BMs is observed, which effectively inhibits cell migration throughout a 14-day experimental period. Furthermore, uniform Col-IV networks are formed between fibroblast layers and endothelial monolayer, indicating the regeneration of natural BMs

in 3D tissues. To demonstrate the advantages of LbL assembly technique on the creation of large-sized and customizable shapes of A-BMs, 3D organized vascular channels have been successfully engineered by the *in-situ* formation of PLL/Dex NFs between layerd of smooth muscle cells (SMCs) layers and a confluent monolayer of ECs. This study provides a guideline for engineering organized 3D tissue models by regulating cell migration. Such models could yield more dependable outcomes for new drug screening, nanotoxicology assessments, and implantation studies.

2. Results and discussion

2.1 Fabrication of PLL/Dex NFs

The LbL assembly technique has been demonstrated to be a highly effective method for the *in-situ* fabrication of shape-customized nanofilms in 3D tissues, which holds significant potential to serve as A-BMs to facilitate compartmentalized co-culture of cells.[32,33] In the present study, PLL and Dex are utilized as foundational components for the construction of positively charged films, as illustrated in **Figure 1a**. PLL is recognized as a well-known polycation, comprising a polypeptide derived from the essential amino acid L-lysine. Dex is characterized as a non-toxic, hydrophilic polysaccharide, consisting of D-glucopyranose repeating units linked through glycosidic linkages. At physiological pH, each repeating unit of PLL carries a positive charge on the amine, whose ζ-potential is measured at 16.7 ± 6.7 mV (**Figure 1b**). Although it is known that Dex have zero net charge, an abundance of uniformly distributed hydroxyl groups in Dex form intermolecular hydrogen bonds with amine and amide groups of PLL.[38] PLL/Dex multilayer nanofilms were fabricated for the first time by alternating deposition of the two polymers through the hydrogen bonds between PLL and Dex (**Figure 1a**), resulting in a net positive surface charge. This assembly process was assessed using a quartz crystal microbalance (QCM). As shown in **Figure S1** (left), a decrease in frequency was observed with each assembly step, suggesting the successful alternate deposition of PLL and Dex. Throughout the assembly process, the variation in film thickness was determined based on the changes in frequency according to Sauerbrey's equation,[39] as recorded by QCM (**Figure 1c**). Upon reaching the assembly of 5 bilayers, the mass of deposited film was approximately 14.2 ± 0.47 nm. In the same way, the electrostatic interaction-driven LbL films comprising PLL and dextran sulfate (PLL/DS), poly(allylamine hydrochloride)/poly(styrene sulfonate) (PAH/PSS) showed clear step-by-step increases

in -Δf. For performance comparison with PLL/Dex films, Col-IV/LM, FN/G, FN/Col-I films were also developed via the specific biological interaction (**Figure 1d**). Furthermore, the morphological characteristics of PLL/Dex NFs were analyzed using atomic force microscopy (AFM), as depicted in **Figure 1e**. AFM image clearly demonstrated the development of a smooth and uniform film with a roughness of 4.08 ± 0.85 nm. Additionally, a fibrous structure accompanied by some granules was observed, indicating the intricate surface details of the films. Hundreds of scratch tests were conducted using an AFM tip in contact mode on a small area (1×1 μm) to measure the thickness of the deposited polymer layers. The thickness of PLL/Dex NFs, defined by the height difference between the scratched and unscratched areas, was approximately 20 nm (**Figure 1f**). The lower value of thickness estimated by QCM from Sauerbrey's equation may be due to the fact that it does not take into account the viscoelasticity of the soft gel-like film in the swollen state, which is usually formed by weak interactions.[40] Moreover, the correlation between the increase in film thickness and the number of assembly steps, as quantified by QCM, illustrates that the film thickness, measured on the nanometer scale, can be easily adjusted. This capability highlights the precision and flexibility of the LbL assembly technique in tailoring nanofilm dimensions to specific requirements.

The nanofilm stability in the physiological environment was also evaluated using QCM at 37 °C. As shown in **Figure S1** (right), upon immersion in PBS, the frequency of assembled PLL/Dex NFs (blue line) initially exhibited a slight increase because of the removal of unabsorbed polymers, as well as the partial disassociation of assembled nanofilms. Then it kept stable and the remaining weight percentage of nanofilm was around 87% after the immersion for 60 min, indicating the stability of assembled PLL/Dex NFs (**Figure 1g**). Conversely, the remaining weight percentage of nanofilm immersed in DMEM/10% FBS exceeded 160% (indicated by the red line), a phenomenon attributable to the gradual attachment of proteins on the film surface. In conclusion, the ability of PLL/Dex NFs to precisely control thickness at the nanoscale combined with their stability in physiological conditions establishes a robust basis for their application as A-BMs in the *in-vitro* construction of 3D tissue structures.

2.2 Cell adhesion on PLL/Dex NFs

Since both endothelial and mesenchymal cells are co-localized nearby and adhere

well to the natural BMs, cell adhesion on the fabricated A-BMs were systematically evaluated. The cell adhesion process involves the interaction between integrins in cell membrane and adhesive proteins on the substrate surface, such as fibronectin (FN). The protein adsorption on the films was therefore investigated in **Figure S2**, which was quantified by QCM. Compared to the Col-IV/LM NFs that demonstrated favorable A-BMs performance and function as reported in our previous study,[32,33] the absorbed amount of both bovine serum albumin (BSA) and FN on PLL/Dex NFs was higher due to the positively charged surface, which will promote the subsequent cell adhesion.[41] The observed low protein adsorption rate on Col-IV/LM NF may be attributed to the synergistic effects of film disassembly, which is influenced by the attraction of proteins in solution, and the subsequent attachment of these proteins. **Figure S3, 4** depict the cell adhesion and spreading morphology on different films including ECM proteins, polyelectrolytes and PLL/Dex films by cytoskeletal staining. Both fibroblast (NHDF) and endothelial cells (HUVEC) adhered well to the cell culture inserts (w/o NFs) and Col-IV/LM NFs owing to the inherently cell-friendly nature of these matrices. Comparable cell spreading results were also observed on PLL/Dex NFs, displaying their characteristic morphologies. In contrast, due to the hydrophilic nature of dextran sulfate, PLL/DS NFs inhibited cell adhesion and spreading, and cells remain heavily aggregated even after two days of incubation, especially HUVEC. Quantitative analysis further demonstrated that PLL/Dex NFs exhibited enhanced cell adhesion properties relative to PLL/DS NFs, thanks to their positively charged surfaces. There was no significant difference in cell spreading area and adhered cell number on PLL/Dex NFs compared to the cell-friendly substrates, highlighting the favorable cell adhesion properties of the prepared PLL/Dex NF.

Furthermore, endothelial cells (ECs) attach tightly and align to BMs, with their function being regulated by these BMs. Functions of ECs on the developed A-BMs was therefore investigated through 2D culture of HUVEC, including the expression of endothelial marker CD31 and tight junction protein, zonula occludens-1 (ZO-1). CD31 is an adherent molecule highly enriched at interendothelial junctions of vascular endothelial cells and is involved in angiogenesis, vascular integrity, and remodeling.[42] ZO-1 is a tight junction protein and plays an important role in the maintenance and regulation of epithelial/endothelial barrier function.[43] **Figure S5** illustrates that in addition to PLL/DS

NFs, a cobblestone-like morphology of HUVEC was observed on all substrates, with no significant differences noted. However, HUVEC displayed poor spreading on PLL/DS NFs due to the inhibitory effect of dextran sulfate on cell attachment. The distribution and margin of both CD31 and ZO-1 were more distinct on Col-IV/LM NFs compared to PLL/Dex NFs or naked insert membrane, because of the role of BM proteins in enhancing endothelial regeneration.[44] Meanwhile, the uniform and continuous signals of CD31 and ZO-1 on the edge of cell-cell joints demonstrated the barrier integrity of an endothelial monolayer culture on PLL/Dex NFs.[45] Overall, the findings concerning cell adhesion and functions of ECs highlight the potential of PLL/Dex NFs as a robust scaffold capable of supporting endothelial and mesenchymal cells. Their nanoscale thickness and stability in physiological environments further provide insights into their suitability as A-BMs in tissue engineering. The subsequent sections will concentrate on thethe barrier properties of the developed A-BMs during the long-term tissue culture.

2.3 Barrier function of LbL films on 3D patterned multicellular co-culture

Tissue engineering has garnered considerable interest for its potential in constructing 3D tissues or organs. While precise control over cell localization in a 3D construct is achievable, maintaining the ordered structure of tissues over time in culture presents challenges due to cell migration. In particular, migration of ECs plays a crucial role in angiogenesis, and they readily migrate toward attractors such as basic fibroblast growth factor secreted by NHDF.[15] Consequently, to replicate the organized and layered tissue structure, where natural BMs are distributed between endothelial (epithelial) cells and connective tissues *in vivo*, PLL/Dex NFs were assembled *in-situ* between fibroblast layers and ECs monolayer (**Figure 2a**). In this section, the barrier effect of PLL/Dex NFs, which act as A-BMs to block ECs migration and maintain 3D patterned multicellular co-cultures, was estimated. Meanwhile, we also compared the barrier effect of other candidate A-BMs, including Col-IV/LM NFs reported in previous studies[32,33] and polyelectrolyte LbL film composed of PLL and dextran sulfate (DS), a biocompatible polyanionic polymer derived from dextran through sulfation.

The developed 3D patterned multicellular structure and the location of PLL/Dex NFs were confirmed by the cross-sectional confocal laser scanning microscopy (CLSM) (**Figure 2b**). Assembled FITC-PLL/TRITC-Dex NFs was observed to locate between the

HUVEC monolayer and the NHDF layers, forming a "sandwich" structure. 3D-constructed CLSM image in **Figure 2c** further verified the distribution of nanofilms between different cells. To develop the A-BMs between different cells, the alternate deposition of PLL and Dex was carried out *in-situ* on NHDF layers. The dipping and washing process with 50 mM of Tris-HCl buffer solution (pH 7.4) for around 2.5 hours might induce the detachment or death of cells due to the absence of glucose. Cell numbers and cell viability were then assessed after 24 hours of culture. As expected, cell counts for samples subjected to LbL assembly were approximately 43% lower than those for the untreated control sample, indicating cell loss during the assembly process (**Figure 2d**). However, there was no difference in cell survival rate with or without dipping assembly, which was approximately 87%. The 13% mortality in all groups was caused by 20 minutes of enzymatic digestion using 0.2% trypsin and 0.1% EDTA during the cell isolation. The biocompatibility of the *in-situ* dipping assembly process for nanofilm fabrication in 3D tissues was further proved by the Live/Dead staining assay in **Figure S6**. Only few dead cells can be observed in each tissue, indicating the mild nature of the assembly process.

During the tissue culture, relative position of HUVEC and NHDF was monitored through CLSM, as shown in **Figure 2d**. Consistent with previous studies,[32] initially, HUVEC monolayer was localized hierarchically on the tissue surface and migrated subsequently into NHDF layers, extending even to the tissue bottom within 3 days in the control group lacking any physical barrier. However, under the barrier effect of A-BMs between HUVEC and NHDF, the migration of HUVEC was effectively prevented within 7 days of co-culture. Moreover, the innermost layer of blood vessel lumen consists of a monolayer of ECs lining the interior surface. These intact ECs attach and align tightly to BMs, forming a squamous confluent layer.[46] A CD31-marked confluent HUVEC monolayer was observed in **Figure 2e**, indicating the formation of a continuous endothelial layer on PLL/Dex NFs. However, in the control sample without A-BMs and in a co-culture system utilizing Col-IV/LM NFs, not only monolayers of HUVEC were found, but also elongated HUVEC and cross-capillary networks. These results are related to migration and sprouting of ECs, and these phenomena are undesirable when constructing well-organized vascular tissues. Migrated HUVEC were also observed in the group containing PLL/DS NFs despite the poor cell adhesion and an incomplete

endothelial layer on PLL/DS NFs. In addition, cross-sectional CLSM images provide substantial evidence of the barrier effect of PLL/Dex NFs in compartmentalized tissue cultures, effectively restricting HUVEC to the tissue surface as depicted in **Figure 2f**. In contrast, ECs migration into NHDF layers was clearly found in the other samples. This migration was further elucidated through a video (**Video S1**), which described the HUVEC movement into NHDF layers within a 3D tissue structure viewed from top to bottom. Histological analyses (**Figure S7**) also confirmed these findings that CD31-marked HUVEC localized on the surface of 3D tissues in the presence of PLL/Dex NFs. But, HUVEC were observed in the middle of 3D tissues, even forming capillary lumen, in the other samples. Considering that BM proteins would be secreted and deposited during the tissue culture for at least 10 days,[34] the long-term patterned culture was investigated. The relative position of HUVEC, as well as the migrated depth (**Figure 2g**, relative position changes of HUVEC compared with their position on Day 0) and migrated cell number (**Figure 2h**), were monitored and quantified over a 14-day co-culture period through the analysis of 3D cross-sectional CLSM images in **Figure S8**. Consistent with the analysis in **Figure 2d**, without any barrier, migrated HUVEC in the control sample was observed on the first day of co-culture. Despite the evidence that Col-IV and LM possess specific cell-binding sites to guide cell adhesion and migration, the inhibitory capacity of Col-IV/LM NFs was limited to a maximum of 3 days. This limitation is due to the fact that these protein membranes are destabilized during co-culture and are subject to enzymatic degradation, rendering them incapable of efficiently regulating cell migration in the long term.[33] On the contrary, the migration of HUVEC was completely inhibited by PLL/Dex NFs, preserving the compartmentalized tissue structure for approximately two weeks. A comparative analysis revealed that negligible cell migration was observed after a 14-day culture due to the barrier effect of PLL/Dex NFs, and the minimal migration depth counted was a result of the cell proliferation-induced changes in tissue thickness. Although PLL/DS NF and PLL/Dex NF were assembled from virtually the same polymers, including polylysine and dextran/derivatives. Moreover, studies have shown that ECs can penetrate dextran methacrylate hydrogels to establish new vascular formations, suggesting that Dex does not inhibit EC migration.[47] Both the number of migrated HUVEC and the depth of their migration were significantly greater in the group treated with PLL/DS NFs in comparison to those treated with PLL/Dex NFs. So here's the question: what exactly is the mechanism by PLL/Dex NFs prevent cell

migration? We'll discuss it in the following section. In summary, through the research discussed above, superior performance of PLL/Dex NFs in preventing HUVEC migration for up to two weeks is confirmed, indicating their potential to act as an effective barrier of A-BMs for compartmentalized tissue culture.

2.4 Effects of the outmost surface charge on cell migration

To investigate why PLL/Dex NFs possess superior performance to both Col-IV/LM NFs and PLL/DS NFs in preventing HUVEC migration, a series of LbL films were constructed for the patterned cell co-culture (**Figure 3**), including polyelectrolyte and ECM protein multilayered films, as well as Matrigel. The LbL films assembly process were recorded by QCM (**Figure S9, 2d**). The cross-sectional CLSM images in **Figure S10** displayed the relative position of GFP-HUVEC (in green) and NHDF (stained with cellTracker deep red) in the presence of ECM protein nanofilms at Day 7. However, these nanofilms, including Col-IV/LM, FN/Col-I, and FN/G, failed to prevent the migration of HUVEC. Only the patterned co-culture structure was maintained with Matrigel coating. Matrigel, derived from Engelbreth-Holm-Swarm tumor BMs, consists of almost the same components as natural BMs but raises safety concerns due to its tumorigenic origin.[48] Further analysis (**Figures 3c, d**) compared the effectiveness of LbL films formed via electrostatic interactions versus those formed via hydrogen bonds. Interestingly, films formed from polycationic and nonionic polymers played a better role in preserving the patterned tissue sturcture than their electrostatically assembled counterparts. This difference in performance appears to be related to the surface ζ-potential of the films, where the effective nanofilms having a positively charged surface and the ineffective ones negatively charged (**Figure 3b**). To further investigate the effects of the outmost surface charge on cell migration, nanofilms starting with DS and ending with PLL (DS/PLL NFs), which presented as positively outmost surface charge, were effective in preventing HUVEC migration, as showin in **Figures 3c** (bottom) & **3e**. Conversely, PLL/DS NFs with negatively charged surfaces were ineffective in blocking HUVEC migration, as discussed above. Additionally, negligible cell migration was found in the presence of both PLL/Dex and Dex/PLL NFs, both of which have positively charged surfaces. The aforementioned data indicate that the composition of these films is not the primary factor inhibiting cell migration and sprouting; rather, the surface charge plays a critical role. This experimental phenomenon can be explained by the findings from Federer group.

They found that apoptotic cells induce ECs sprouting through the phenotypic expression of a negatively charged membrane surface.[35] They proposed a concept, based on their observations, that sprouting cells exhibit a strongly positively charged surface, as evidenced by the binding of anionized ferritin to sprouting ECs. While the exact source and nature of this positive surface charge on ECs during sprouting remain unclear, these observations are consistent with studies that ECs tend to elongate and migrate toward the cathode in a direct current electric field.[36,37] Their hypothesis is also supported well by our findings that the application of positively charged nanofilms inhibits the migration or elongation process of HUVEC, despite the fact that HUVEC itself tends to sprout in response to basic fibroblast growth factor secreted by the underlying NHDF.[49] These positively charged nanofilms permitted compartmentalized co-culture of fibroblasts and ECs, acting like a barrier, suggesting that they have the potential to serve as A-BMs for the construction of highly organized 3D vascular tissues.

2.5 Regeneration of natural BMs

Natural BMs are supposed to deposit between different cells to fulfill their role in supporting and maintaining the integrity and organization of tissue structures, while ensuring the compartmentalized multicellular co-culture and enabling engineered tissues to mimic the complex functions of native tissues.[34] Col-IV and LM are identified as the primary components of BMs, and are secreted during tissue culture. Therefore, the deposition of Col-IV was evaluated over 7 days in 3D tissues (**Figure 4a**). To avoid the interference of exogenous Col-IV, a coating of LM was applied instead of using Col-IV/LM NFs. Deposited Col-IV was observed to be mainly distributed between HUVEC monolayer and NHDF layers (**Figure 4b**), forming dense fibrous networks. However, beneath the monolayer of HUVEC, the fluorescence signals of Col-IV were also detected in the samples without A-BMs or with LM coating, especially around the capillary lumen structure, as shown around the white arrows in **Figure 4c**. Moreover, the LM coating generally enhances cell adhesion and growth, subsequently facilitating the secretion of Col-IV. The fluorescence intensity of Col-IV in the sample consisting of PLL/Dex NFs was slightly lower, but still comparable to the sample with LM coating (**Figure S11**). There was no significant difference among the three samples. Taken together, these findings confirm the deposition of Col-IV in the presence of the PLL/Dex NFs barrier, suggesting the regeneration of natural BM in the long-term, organized tissue culture.

2.6 3D patterned vascular structure

Biological systems display inherent hierarchical structures, as illustrated by the specialized tubular architecture of blood vessels, comprised of ECs, smooth muscle cells (SMCs), and adjacent connective tissues. Typically, in the vasculature, BMs provide foundational support to the endothelial lining and are closely associated with SMCs.[50] The precise mimicking of these structural is crucial for the wide applications of engineered tissue models. In this section, 3D patterned vascular structure was engineered through the sequential seeding of SMCs and ECs within tubular microchannels, constructed using sacrificial templating methods. PLL/Dex NFs were *in-situ* assembled between ECs and SMCs, functioning as A-BMs to preserve the organized architecture. As shown in **Figure 5a & S12**, thermoresponsive poly(2-cyclopropyl-2-oxazoline) (P*cyclo*PrOx) scaffolds, fabricated via melt electrowriting (MEW) as detailed in previous study,[51] were embedded in fibrin gel stabilized in a bioreactor. These scaffolds were then dissolved in cold PBS, resulting in the formation of interconnected microchannels, measuring 30 mm in length and 300 µm in diameter (**Figure S13**). In **Figure 5b & S14a**, the full extension and coverage of AoSMC with a spindle-shaped elongated morphology was confirmed, and a confluent endothelial monolayer was also found on the inner side of the microchannel. Following the alignment of AoSMC, LbL assembly of PLL and Dex was carried out in the circular microchannel to form A-BMs on the AoSMC layer, followed by the seeding of HUVEC on these films (**Figure 5c**). CLSM image in **Figure 5d** (right) displays a clear tubular double-layered vascular structure in the presence of PLL/Dex NFs, which was composed of an outer AoSMC layer and inner confluent HUVEC layer (**Figure 5e & S15**). **Video S2** also clear shows the 3D patterned circular vascular structure. Although no migration of HUVEC was observed during the tissue culture, this may be due to the fact that the AoSMC attached in microchannels were almost monolayer. In **Figure S16**, during layered co-culture of SMCs and ECs performed in the 24-well insert, the cross-sectional CLSM images demonstrate that in the absence of PLL/Dex NFs, migration and sprouts of HUVEC were observed, while patterned structure of HUVEC and AoSMC was maintained with the assistance of A-BMs. Furthermore, without the support of PLL/Dex NFs, the HUVEC monolayer in direct contact with the underlying AoSMC was unstable and proned to detach from the AoSMC layer and formed aggregates, leading to microchannel blockage (**Figure 5d** (left), **Figure**

S14b). This observation suggests the critical role of PLL/Dex NFs, serving asA-BMs, in providing a supportive platform essential for preserving the integrity and stability of the vascular structure.

3. Conclusion

In conclusion, positively charged multilayer nanofilms, fabricated through LbL assembly of PLL and Dex, effectively recapitulate the barrier properties of BMs, successfully inhibiting the migration and sprouting of HUVEC. PLL/Dex NFs were utilized as scaffolds for cell culture, where endothelial cells demonstrated typical cobblestone morphology and barrier functions, evidenced by the expression of tight junctions comparable to those observed on cell-friendly substrates. Compared to the previously reported A-BMs composed of Col-IV/LM NFs, the newly developed A-BMs demonstrate significantly enhanced barrier properties. They effectively inhibite HUVEC migration over 14 days that matches the regeneration timeline of natural BMs in 3D tissues.[34] Through systematic comparative analysis, it was determined that the improved barrier functions of the nanofilms could be attributed to their positive surface charge, which played a crucial role in inhibiting HUVEC migration or sprouting. This observation is corresponds to previous reports that sprouting endothelial cells (ECs) possess a poritvely charged surface and typically migrate towards the cathode in a direct current electric field.[35–37] Furthermore, the easy and biocompatible assembly process enables the creation of large-sized and customizable shapes of A-BMs for on-demand construction of organized tissue models for the understanding of integrated biological systems and ultimately the development of regenerative therapeutics. As an example, a 3D patterned vascular structure with clear lumen was engineered in a microchannel created in fibrin gel by sacrificial template method. Positioned between SMCs layers and ECs monolayer, PLL-Dex NFs were *in-situ* assembled fowllowing the topography of microchannel to support the patterned cell co-culture.

4. Experimental section

4.1 PLL/Dex multilayered nanofilm fabrication and characterization

A 27 MHz quartz crystal microbalance (QCM, AFFINIX Q8, ULVAC SHOWCASE, Kanagawa, Japan) was used to quantitatively analyze the LbL assembly of α-poly-L-

lysine (PLL, Mw 15000-30000, 167-12671, FUJIFILM Wako, Osaka, Japan) and dextran (Dex, Mw 60000, FUJIFILM Wako, Osaka, Japan) on a gold-coated quartz crystal sensor as previous reported protocols.[32,52–54] First, QCM electrodes were cleaned with piranha solution (fresh mixture of H_2SO_4/40% H_2O_2 aqueous solution=3:1 (v/v)) for 3 min, three times. Prior to use, QCM electrodes were rinsed with Milli Q and dried with N_2. Temperature was maintained at 37 °C in all experiments. For the QCM study of film formation, PLL was coated as the first layer and Dex was deposited subsequently. For each deposition step, 100 μL of 50 mM Tris-HCl buffer solution (pH 7.4) was first added to each well. Under gentle stirring by the automatic stirring rod, 5 μL of polymer solutions (2 wt% in 50 mM Tris-HCl buffer) were gently added to each well and the frequency was recorded real-timely. Each adsorption duration was 15 min until the equilibrium. Between each step, washing the electrodes with 1 mM Tris-HCl buffer solution (pH=7.4) for three times to remove excess and non-absorbed polymers. The alternate steps were repeated until 5 bilayers, and the developed nanofilm was denoted as PLL/Dex NFs. The deposited amount of each polymer in each step was calculated referring to the Sauerbrey equation: $-\Delta F\ (Hz) = 0.63\ \Delta m\ (ng/cm^2)$.[39,55] Other multilayered films were also fabricated using the methods described above. And for the characterization, multilayered films were assembled on glass substrates.

4.2 AFM investigation

The prepared PLL/Dex multilayered nanofilms on glass substrate were air-dried, and the samples were subsequently imaged using atomic force microscopy (AFM) in tapping mode under ambient conditions. For imaging the topographical surface of the nanofilms, highly doped silicon cantilevers coated with gold (PPP-NCSTAuD, NANOSENSORS™, Neuchatel, Switzerland), featuring a resonant frequency of 160 kHz and a nominal spring constant of 7.4 N/m, were utilized.

Thickness measurements were preformed using a AFM tip-scratch method.[56–58] Briefly, a small square area (1.0 × 1.0 μm) was scanned in the contact mode to eliminate the deposits without causing damage to the glass substrate. Subsequently, a larger window (10 × 10 μm) was examined in tapping mode to ascertain the height differential, which corresponds to the actual thickness of the nanofilms. Notably, the depth of the scratches increased proportionally with the duration of the scratching process, until a point was reached where no further changes were observed.

4.3 Evaluation of stability and protein adsorption

The investigation of the stability and protein adsorption of multilayered nanofilms was conducted using QCM analysis. After the assembly of PLL/Dex NFs on QCM electrodes, the quantification of bovine serum albumin (BSA, 9048-46-8, Sigma, St. Louis, USA) and fibronectin (FN, 289-149-2, Sigma) adsorption was performed using the QCM frequency shift, as detailed above. Similarly, the stability was assessed by immersing the assembled nanofilms in both PBS and DMEM medium supplemented with 10% FBS for over 1 hour to monitor the frequency changes using QCM.

4.4 Surface ζ potential

Multilayered films were assembly on glass substrates (4 mm × 5 mm) following aforesaid assembly conditions. Their surface ζ potential was evaluated via phase analysis light scattering that has been previously described by Corbett.[59,60] Briefly, glass substrates coated with the prepared nanofilms were stabilized on a holder positioned between electrodes and then submerged in a ZEN1020 plate cell (Surface zeta potential cell, Malvern Panalytical), containing a solution of narrowly dispersed tracer particles. The velocity of the tracer particles, under the influence of an alternating current (AC) field, is quantified through phase analysis light scattering. The overall velocity of the tracer particles at different positions results from the combined impact of particle electrophoretic migration and electro-osmotic flow in the vicinity of the solid-liquid interface. As the testing position moves farther away from the sample surface, the influence of electro-osmotic flow diminishes, eventually reaching a point where the observed mobility is solely a result of electrophoretic migration. The obtained values are graphed as a function of surface displacement, and the surface ζ potential is determined by extrapolating the data to zero-displacement. The contribution arising exclusively from the surface ($\zeta_{surface}$) is calculated from the equation $\zeta_{surface}$ = -intercept + $\zeta_{particle}$. The surface ζ potential of multilayered nanofilms was evaluated using Zetasizer nano ZS. 250 nm of Nile Red-polystyrene nanoparticles (0.0005% w/v, FP-0256-2, Spherotech Inc, Lake Forest, USA) in 50 mM Tris-HCl buffer solution (pH 7.4, r.t.) were used as tracer particle. Mobility measurements were carried out at distances of 125, 250, 375, 500, and 1000 μm away from the sample surface.

4.5 Cell culture

Normal human dermal fibroblast cells (NHDF, CC-2509) (Passage: 5-8) were cultured with dulbecco's modified eagle medium (DMEM) supplemented with 10% fetal bovine serum (FBS) and 1% penicillin/streptomycin, in an atmosphere containing 5% CO_2 at 37 °C. Human umbilical vein endothelial cells (HUVEC, C2517A) (Passage: 5-6) and GFP expressed HUVEC (GFP-HUVEC, Argio-Proteomie, Massachusetts, USA) (Passage: 5-6) were cultured in endothelial cell growth medium-2 (EGM-2, CC-3162). Human aortic smooth muscle cells (AoSMC, CC-2571) (Passage: 2-3) were cultured in smooth muscle cell growth medium-2 (SmGM-2, CC-3182). For tissue culture, mixed culture media were used: DMEM/EGM-2 (1:1, v:v) for the co-culture of NHDF and HUVEC, SmGM-2/EGM-2 (1:1, v:v) for the co-culture of AoSMC and HUVEC. All medium and cell were purchased from Lonza, Basel, Switzerland.

4.6 Evaluation of cell adhesion and cell functions on multilayered nanofilms

Various nanofilms were assembled on the membrane of 24-well inserts. 1.0×10^5 of NHDF and HUVEC were seeded respectively on the nanofilms, and a blank insert membrane served as the control group. Both NHDF and HUVEC were cultured for 24, 48 h and the cytoskeleton was stained to examine the morphology of adhered cells. Furthermore, HUVEC were cultured for a period of 5 days to analyze the expression of CD31 and ZO-1.

4.7 Construction of patterned 3D cell co-culture structure

PLL/Dex NFs were engineered to reside between fibroblast layers and endothelial cells, creating a “sandwich” configuration that mimics the architecture of natural tissue. Specifically, 250 μL of 1.0×10^6 NHDF suspension were seeded into a 24-well insert that had been pre-incubated in a laminin (40 μg/mL)/Tris-HCl solution (50 mM, pH=7.4) at 37 °C for 1 hour to facilitate cell adhesion. 1 mL of DMEM was added to the underlayer of the transwell and the samples were then placed in an incubator at 37 °C for 24 hours to allow NHDF attachment. After three washes with PBS, 250 μL of PLL and Dex (0.1 wt%)/Tris-HCl (50 mM, pH 7.4) solutions were sequentially added to the insert, with each addition followed by an incubation at 37 °C for 15 min. 1 mL of Tris-HCl buffer solution was maintained beneath the inserts. Following each step, the samples were rinsed once with a 1 mM Tris-HCl buffer solution to eliminate excess and non-adsorbed

polymers. This alternating adsorption process was repeated five times, leading to the formation of $(PLL/Dex)_5$ nanofilms. A volume of 250 μL of 1.0×10^5 HUVEC suspension in mixed medium (DMEM/EGM-2 at a 1:1 ratio) was placed on the assembled nanofilms, and 1 mL of the mixed medium was added into the underlayer of the transwell. The samples were then incubated for 24 hours to facilitate HUVEC adhesion, after which the medium was replaced with 2 mL of mixed medium per well. The tissues were cultured for a period ranging from 5 to 21 days, with the medium being replaced once every two days. A patterned cell co-culture structure, lacking of nanofilms, served as the control sample. The efficacy of cell separation between NHDF and HUVEC using $(Col\text{-}IV/LM)_5$ nanofilms was evaluated and compared to that achieved with PLL/Dex nanofilms. To determine the precise locations of both NHDF and HUVEC, immunofluorescence staining and histological staining techniques were employed.

To verify the integrity of this patterned structure, fluorescein isothiocyanate (FITC) labeled PLL (Mw 15000-30000, P3543-10MG, Sigma) and tetramethylrhodamine (TRITC)-Dex (Mw 500000, 52194-1G, Sigma) were incorporated between the layers of NHDF and HUVEC. In conjunction with immunofluorescence staining of NHDF and HUVEC, the fluorescent PLL/Dex nanofilms were visualized using confocal laser scanning microscope (CLSM, FV3000, Olympus, Japan).

4.8 Fabrication of tubular multicellular structure in 3D hydrogel

Vascular-like structure was constructed in 3D fibrin gel as previous publication with modifications.[51] Glass coverslips (D: 25 mm) were pasted to the bottom of bioreactor using double-side tapes. Templating scaffold of poly(2-cyclopropyl-2-oxazoline) (P*cyclo*PrOx) with a diameter 500 μm was placed on the saddle supports of the bioreactors and then fixed with P*cyclo*PrOx solution (15wt%). Following adhesive drying at ambient temperature, bioreactors with P*cyclo*PrOx scaffolds were sterilized under UV light for 10 min. Then, 400 μL of fibrin gel was used to fill the main chamber of bioreactor and the scaffolds were embedded in the fibrin gel. Fibrin gel was prepared by mixing 266.7 μL of 10wt% fibrinogen solution (F8630-5G, Sigma Aldrich, St. Louis, USA) and 133.3 μL of 50 U/mL thrombin solution (E6758-500G, Sigma Aldrich, St. Louis, USA) at room temperature and then incubated at 37 °C for the complete gelation. Once the hydrogel formed, PBS solution was added to the bioreactor chambers to dissolve the P*cyclo*PrOx scaffold, leaving empty microchannels.

10 μL of 3.0×10^5 AoSMC suspension were injected to the microchannel that was pre-incubated in fibronectin solution (0.01wt%) at 37 °C for 1 hour to facilitate cell adhesion. Following cell seeding, the bioreactor was transferred to incubator. After 3 hours incubation, bioreactor was turned upside down and incubated for another 3 hours to ensure the homogeneity of the cell attachment. 1.0 mL of SmGM-2 was added to each side chamber and 0.5 mL SmGM-2 was added in the main chamber. Cell attachment was confirmed by cytoskeleton staining of AoSMC after 2 days culture. HUVEC was also seeded following the same protocol, but the incubation time after injecting cell suspension was 15 min for each side. Confluent HUVEC monolayer attached in the microchannel was confirmed by CD31 staining after 5 days culture. Tubular multicellular structure was fabricated by seeding AoSMC and HUVEC successively. Briefly, AoSMC was seeded and cultured for 2 days, and then *in-situ* LbL assembly of PLL/Dex NFs was performed on AoSMC surface before HUVEC seeding. After that, mixed medium (SmBM/EGM at 1:1 ratio) was used for tissue culture. The medium was changer every day.

4.9 Regeneration of natural BMs

To assess the secretion of collagen type IV (Col-IV) by cells co-cultured with PLL/Dex nanofilms, immunofluorescence staining for Col-IV was conducted and subsequently analyzed using the FV3000 microscope. A control sample consisting of patterned cell co-culture without nanofilms was carried out for comparison. Laminin coating (0.004 wt% in 50 mM Tris-HCl) was applied between NHDF and HUVEC layers instead of Col-IV/LM nanofilms to compare distribution of naturally deposited Col-IV with those cultured with PLL/Dex nanofilms. The patterned tissues were cultured for 7 days, followed by staining with anti-Col-IV and anti-CD31 antibodies, and the morphology of Col-IV networks was visualized using the FV3000 microscope.

4.10 Cell tracker staining

Cell Tracker™ deep red (C34565, Invitrogen, California, USA) was initially prepared in dimethyl sulfoxide (DMSO) at 10 mM and subsequently diluted to a 1:1000 volume ratio in FBS-free medium. Pre-cultured cells underwent three PBS washes before a 40-minute incubation with the dye at 37 °C. Following aspiration of the dye-containing medium and three additional PBS washes, the cells were incubated in DMEM at 37 °C for a minimum of 24 hours prior to detachment.

4.11 Immunofluorescence staining

2D monolayer or 3D tissues cultured in 24-well insert were rinsed three times with PBS and fixed by 4% paraformaldehyde (Fujifilm Wako, Osaka, Japan) for 15 min at room temperature. Following by PBS rinsing for three times, permeabilization was then carried out using 0.2% Triton-X 100 (Sigma-Aldrich, St. Louis, MO, USA) for 30 min at room temperature. After PBS rinsing, 1wt% BSA/PBS solution was added at room temperature for 30 min to block the unspecific staining of the antibody. The samples were then incubated with primary antibodies overnight at 4 °C: TRITC-phallotoxin (084K0443, Sigma, St. Louis, USA) and anti-CD31 antibody (mouse anti-human, NCL-CD31-1A10, Leica, Wetzlar, Germany; anti-rabbit, ab28364, abcam, Cambridge, UK) were diluted in 1% BSA in PBS at 1/100, while anti-ZO-1 (mouse anti-human, ZO1-1A12, Invitrogen, Waltham, MA, USA), anti-collagen-IV (monoconal mouse anti-human, clone CIV 22, Thermo Fisher Scientific, Waltham, MA, USA) were diluted in 1% BSA in PBS at 1/50. After rinsing with PBS for three times, samples were then incubated for 2 hours at room temperature in the dark with secondary antibodies diluted at 1/200 in 1% BSA in PBS: goat anti-mouse, Alexa Fluor 488 (A11001), Alexa Fluor 546 (A11003), Alexa Fluor 647 (A21235) (Thermo Fisher Scientific, Waltham, MA, USA), and goat anti-rabbit, Alexa Fluor 488 (ab150077, Abcam, Cambridge, UK). The nuclei were stained with Hoechst 33342 (H3570, Thermo Fisher Scientific, Waltham, MA, USA) that was diluted 1000 times in PBS. After staining, the samples were washed with PBS three times. Fluorescence images were then observed with FV3000. Images were digitized using Imaris software (ver. 9.2.1, Oxford Instruments, Bitplane, Belfast, UK). Adhered cell number, coverage area, expression of CD31 and ZO-1, as well as the migrated cell number, depth, were quantified using ImageJ.

4.12 Histology staining

Insert cultured tissues were rinsed with PBS three times and fixed in 4 % PFA for 15 min at room temperature. Another three washes with PBS were performed, and the tissues were then sent to the Applied Research Company for paraffin embedding. Sectional samples were stained with hematoxylin and eosin (H&E) and CD31. Brightfield images were captured using an FL Evos Auto microscope (Thermo Fisher Scientific, MA, USA).

4.13 Cell viability

Trypan Blue stain kit. After the LbL assembly process performed on NHDF layers *in-situ*, incubating the tissues for 24 hours. On the second day, the samples were rinsed with PBS and subsequently incubated in 200 µL of 0.025% trypsin with 0.01 % EDTA at 37 °C for 20 min. During the digestion, pipetting the digested tissues gently twice for the cell isolation. Equivalent amount of mixed medium was added to stop the digestion process. Isolated cells were stained with 0.4% trypan blue (2420718, Thermo Fisher Scientific, Waltham, MA, USA) to quantify the cell number. Live and dead cell number was counted by automated cell counter (Countess II, Thermo Fisher, Waltham, USA).

LIVE/DEAD Viability Assay. Same with the trypan blue stain kit, tissues cultured on the next day were rinsed with PBS for three times and incubated in 250 µL of PBS solution containing Calcein AM and EthD-1/PBS (2 µmol/L) at 37 °C for 45 min in the dark. Cell conditions were imaged at the surface, middle and bottom of the 3D tissue using a FV3000.

Statistical analysis

In this study, all values are presented as means ± standard deviation (SD). Statistical analysis of the data was performed with Student's t-test when more than two samples were compared. Error bars represent standard deviations. Test gave p values considered significant if *p <0.05.

Supporting Information

Supporting Information is available from the Wiley Online Library or from the author.

Acknowledgements

The authors acknowledge financial support Grant-in-Aid for JSPS Research Fellow 202112833.

Conflict of interest

The authors declare no conflict of interest.

Data Availability Statement

The data that support the findings of this study are available from the corresponding author upon reasonable request

Received: ((will be filled in by the editorial staff))

Revised: ((will be filled in by the editorial staff))

Published online: ((will be filled in by the editorial staff))

References

(1) Primo, G. A.; Mata, A. 3D Patterning within Hydrogels for the Recreation of Functional Biological Environments. *Advanced Functional Materials* **2021**, *31* (16), 2009574. https://doi.org/10.1002/adfm.202009574.

(2) Gaspar, V. M.; Lavrador, P.; Borges, J.; Oliveira, M. B.; Mano, J. F. Advanced Bottom-Up Engineering of Living Architectures. *Advanced Materials* **2020**, *32* (6), 1903975. https://doi.org/10.1002/adma.201903975.

(3) Louis, F.; Sowa, Y.; Irie, S.; Higuchi, Y.; Kitano, S.; Mazda, O.; Matsusaki, M. Injectable Prevascularized Mature Adipose Tissues (iPAT) to Achieve Long-Term Survival in Soft Tissue Regeneration. *Advanced Healthcare Materials* **2022**, *11* (23), 2201440. https://doi.org/10.1002/adhm.202201440.

(4) Correia, C. R.; Bjørge, I. M.; Zeng, J.; Matsusaki, M.; Mano, J. F. Liquefied Microcapsules as Dual-Microcarriers for 3D+3D Bottom-Up Tissue Engineering. *Advanced Healthcare Materials* **2019**, *8* (22), 1901221. https://doi.org/10.1002/adhm.201901221.

(5) Sivaraj, D.; Chen, K.; Chattopadhyay, A.; Henn, D.; Wu, W.; Noishiki, C.; Magbual, N. J.; Mittal, S.; Mermin-Bunnell, A. M.; Bonham, C. A.; Trotsyuk, A. A.; Barrera, J. A.; Padmanabhan, J.; Januszyk, M.; Gurtner, G. C. Hydrogel Scaffolds to Deliver Cell Therapies for Wound Healing. *Frontiers in Bioengineering and Biotechnology* **2021**, *9*.

(6) Chandra, P. K.; Soker, S.; Atala, A. Chapter 1 - Tissue Engineering: Current Status and Future Perspectives. In *Principles of Tissue Engineering (Fifth Edition)*; Lanza, R., Langer, R., Vacanti, J. P., Atala, A., Eds.; Academic Press, 2020; pp 1–35. https://doi.org/10.1016/B978-0-12-818422-6.00004-6.

(7) Singhvi, R.; Kumar, A.; Lopez, G.; Stephanopoulos, G.; Wang, D.; Whitesides, G.; Ingber, D. Engineering Cell Shape and Function. *Science* **1994**, *264* (5159), 696–698. https://doi.org/10.1126/science.8171320.

(8) Wu, C.-C.; Reinhoudt, D. N.; Otto, C.; Subramaniam, V.; Velders, A. H. Strategies for Patterning Biomolecules with Dip-Pen Nanolithography. *Small* **2011**, *7* (8), 989–1002. https://doi.org/10.1002/smll.201001749.

(9) Ganjian, M.; Modaresifar, K.; Rompolas, D.; Fratila-Apachitei, L. E.; Zadpoor, A. A. Nanoimprinting for High-Throughput Replication of Geometrically Precise Pillars in

Fused Silica to Regulate Cell Behavior. *Acta Biomaterialia* **2022**, *140*, 717–729. https://doi.org/10.1016/j.actbio.2021.12.001.
(10) Michel, R.; Lussi, J. W.; Csucs, G.; Reviakine, I.; Danuser, G.; Ketterer, B.; Hubbell, J. A.; Textor, M.; Spencer, N. D. Selective Molecular Assembly Patterning: A New Approach to Micro- and Nanochemical Patterning of Surfaces for Biological Applications. *Langmuir* **2002**, *18* (8), 3281–3287. https://doi.org/10.1021/la011715y.
(11) Lu, Y.-C.; Song, W.; An, D.; Kim, B. J.; Schwartz, R.; Wu, M.; Ma, M. Designing Compartmentalized Hydrogel Microparticles for Cell Encapsulation and Scalable 3D Cell Culture. *J. Mater. Chem. B* **2015**, *3* (3), 353–360. https://doi.org/10.1039/C4TB01735H.
(12) Yoshida, S.; Takinoue, M.; Onoe, H. Compartmentalized Spherical Collagen Microparticles for Anisotropic Cell Culture Microenvironments. *Adv. Healthcare Mater.* **2017**, *6* (8), 1601463. https://doi.org/10.1002/adhm.201601463.
(13) Liu, Z.; Nan, H.; Jiang, Y.; Xu, T.; Gong, X.; Hu, C. Programmable Electrodeposition of Janus Alginate/Poly-L-Lysine/Alginate (APA) Microcapsules for High-Resolution Cell Patterning and Compartmentalization. *Small* **2022**, *18* (10), 2106363. https://doi.org/10.1002/smll.202106363.
(14) Piantino, M.; Kang, D.-H.; Furihata, T.; Nakatani, N.; Kitamura, K.; Shigemoto-Mogami, Y.; Sato, K.; Matsusaki, M. Development of a Three-Dimensional Blood-Brain Barrier Network with Opening Capillary Structures for Drug Transport Screening Assays. *Materials Today Bio* **2022**, *15*, 100324. https://doi.org/10.1016/j.mtbio.2022.100324.
(15) Son, J.; Hong, S. J.; Lim, J. W.; Jeong, W.; Jeong, J. H.; Kang, H.-W. Engineering Tissue-Specific, Multiscale Microvasculature with a Capillary Network for Prevascularized Tissue. *Small Methods* **2021**, *5* (10), 2100632. https://doi.org/10.1002/smtd.202100632.
(16) Tavana, H.; Mosadegh, B.; Takayama, S. Polymeric Aqueous Biphasic Systems for Non-Contact Cell Printing on Cells: Engineering Heterocellular Embryonic Stem Cell Niches. *Adv. Mater.* **2010**, *22* (24), 2628–2631. https://doi.org/10.1002/adma.200904271.
(17) M, M. P. Basement Membrane Proteins: Structure, Assembly, and Cellular Interactions. *Critical Reviews in Biochemistry and Molecular Biology* **1992**, *27* (1–2), 93–127. https://doi.org/10.3109/10409239209082560.
(18) Schittny, J. C.; Yurchenco, P. D. Basement Membranes: Molecular Organization and Function in Development and Disease. *Current Opinion in Cell Biology* **1989**, *1* (5), 983–988. https://doi.org/10.1016/0955-0674(89)90069-0.
(19) Pozzi, A.; Yurchenco, P. D.; Iozzo, R. V. The Nature and Biology of Basement Membranes. *Matrix Biology* **2017**, *57–58*, 1–11. https://doi.org/10.1016/j.matbio.2016.12.009.
(20) Yurchenco, P. D. Basement Membranes: Cell Scaffoldings and Signaling Platforms. *Cold Spring Harbor Perspectives in Biology* **2011**, *3* (2), a004911–a004911. https://doi.org/10.1101/cshperspect.a004911.

(21) Hohenester, E.; Yurchenco, P. D. Laminins in Basement Membrane Assembly. *Cell Adhesion & Migration* **2013**, *7* (1), 56–63. https://doi.org/10.4161/cam.21831.
(22) LeBleu, V. S.; MacDonald, B.; Kalluri, R. Structure and Function of Basement Membranes. *Exp Biol Med (Maywood)* **2007**, *232* (9), 1121–1129. https://doi.org/10.3181/0703-MR-72.
(23) Suzuki, S.; Nishiwaki, K.; Takeoka, S.; Fujie, T. Large-Scale Fabrication of Porous Polymer Nanosheets for Engineering Hierarchical Cellular Organization. *Adv. Mater. Technol.* **2016**, *1* (6), 1600064. https://doi.org/10.1002/admt.201600064.
(24) Kim, H. J.; Huh, D.; Hamilton, G.; Ingber, D. E. Human Gut-on-a-Chip Inhabited by Microbial Flora That Experiences Intestinal Peristalsis-like Motions and Flow. *Lab Chip* **2012**, *12* (12), 2165. https://doi.org/10.1039/c2lc40074j.
(25) Jain, P.; Nishiguchi, A.; Linz, G.; Wessling, M.; Ludwig, A.; Rossaint, R.; Möller, M.; Singh, S. Reconstruction of Ultra-Thin Alveolar-Capillary Basement Membrane Mimics. *Advanced Biology* **2021**, *5* (8), 2000427. https://doi.org/10.1002/adbi.202000427.
(26) Gadalla, D.; Tchoukalova, Y. D.; Lott, D. G. Regenerating Airway Epithelium Using Fibrous Biomimetic Basement Membranes. *Journal of Biomedical Materials Research Part A* **2022**, *110* (6), 1251–1262. https://doi.org/10.1002/jbm.a.37371.
(27) Nishiguchi, A.; Singh, S.; Wessling, M.; Kirkpatrick, C. J.; Möller, M. Basement Membrane Mimics of Biofunctionalized Nanofibers for a Bipolar-Cultured Human Primary Alveolar-Capillary Barrier Model. *Biomacromolecules* **2017**, *18* (3), 719–727. https://doi.org/10.1021/acs.biomac.6b01509.
(28) Dohle, E.; Singh, S.; Nishigushi, A.; Fischer, T.; Wessling, M.; Möller, M.; Sader, R.; Kasper, J.; Ghanaati, S.; Kirkpatrick, C. J. Human Co- and Triple-Culture Model of the Alveolar-Capillary Barrier on a Basement Membrane Mimic. *Tissue Engineering Part C: Methods* **2018**, *24* (9), 495–503. https://doi.org/10.1089/ten.tec.2018.0087.
(29) Rossi, A.; Wistlich, L.; Heffels, K.-H.; Walles, H.; Groll, J. Isotropic Versus Bipolar Functionalized Biomimetic Artificial Basement Membranes and Their Evaluation in Long-Term Human Cell Co-Culture. *Adv. Healthcare Mater.* **2016**, *5* (15), 1939–1948. https://doi.org/10.1002/adhm.201600224.
(30) Decher, G.; Hong, J.-D. Buildup of Ultrathin Multilayer Films by a Self-Assembly Process, 1 Consecutive Adsorption of Anionic and Cationic Bipolar Amphiphiles on Charged Surfaces. *Makromolekulare Chemie. Macromolecular Symposia* **1991**, *46* (1), 321–327. https://doi.org/10.1002/masy.19910460145.
(31) Decher, G. Fuzzy Nanoassemblies: Toward Layered Polymeric Multicomposites. *Science* **1997**, *277* (5330), 1232–1237. https://doi.org/10.1126/science.277.5330.1232.
(32) Zeng, J.; Sasaki, N.; Correia, C. R.; Mano, J. F.; Matsusaki, M. Fabrication of Artificial Nanobasement Membranes for Cell Compartmentalization in 3D Tissues. *Small* **2020**, 1907434. https://doi.org/10.1002/smll.201907434.
(33) Zeng, J.; Correia, C. R.; Mano, J. F.; Matsusaki, M. In Situ Cross-Linking of Artificial Basement Membranes in 3D Tissues and Their Size-Dependent Molecular

Permeability. *Biomacromolecules* **2020**, acs.biomac.0c01155. https://doi.org/10.1021/acs.biomac.0c01155.
(34) Furuyama, A.; Mochitate, K. Assembly of the Exogenous Extracellular Matrix during Basement Membrane Formation by Alveolar Epithelial Cells in Vitro. *Journal of Cell Science* **2000**, *113* (5), 859–868. https://doi.org/10.1242/jcs.113.5.859.
(35) Weihua, Z.; Tsan, R.; Schroit, A. J.; Fidler, I. J. Apoptotic Cells Initiate Endothelial Cell Sprouting via Electrostatic Signaling. *Cancer Research* **2005**, *65* (24), 11529–11535. https://doi.org/10.1158/0008-5472.CAN-05-2718.
(36) Li, X.; Kolega, J. Effects of Direct Current Electric Fields on Cell Migration and Actin Filament Distribution in Bovine Vascular Endothelial Cells. *Journal of Vascular Research* **2002**, *39* (5), 391–404. https://doi.org/10.1159/000064517.
(37) Cunha, F.; Rajnicek, A. M.; McCaig, C. D. Electrical Stimulation Directs Migration, Enhances and Orients Cell Division and Upregulates the Chemokine Receptors CXCR4 and CXCR2 in Endothelial Cells. *J Vasc Res* **2019**, *56* (1), 39–53. https://doi.org/10.1159/000495311.
(38) Zeini, D.; Glover, J. C.; Knudsen, K. D.; Nyström, B. Influence of Lysine and TRITC Conjugation on the Size and Structure of Dextran Nanoconjugates with Potential for Biomolecule Delivery to Neurons. *ACS Appl. Bio Mater.* **2021**, *4* (9), 6832–6842. https://doi.org/10.1021/acsabm.1c00544.
(39) Sauerbrey, G.Z. Use of quartz vibration for weighing thin films on a microbalance. *Phys.* **1959**, *155*, 206.
(40) Nishiguchi, A.; Matsusaki, M.; Akashi, M. Structural and Viscoelastic Properties of Layer-by-Layer Extracellular Matrix (ECM) Nanofilms and Their Interactions with Living Cells. *ACS Biomaterials Science & Engineering* **2015**, *1* (9), 816–824. https://doi.org/10.1021/acsbiomaterials.5b00188.
(41) Metwally, S.; Stachewicz, U. Surface Potential and Charges Impact on Cell Responses on Biomaterials Interfaces for Medical Applications. *Materials Science and Engineering: C* **2019**, *104*, 109883. https://doi.org/10.1016/j.msec.2019.109883.
(42) Wimmer, I.; Tietz, S.; Nishihara, H.; Deutsch, U.; Sallusto, F.; Gosselet, F.; Lyck, R.; Muller, W. A.; Lassmann, H.; Engelhardt, B. PECAM-1 Stabilizes Blood-Brain Barrier Integrity and Favors Paracellular T-Cell Diapedesis Across the Blood-Brain Barrier During Neuroinflammation. *Frontiers in Immunology* **2019**, *10*.
(43) Tornavaca, O.; Chia, M.; Dufton, N.; Almagro, L. O.; Conway, D. E.; Randi, A. M.; Schwartz, M. A.; Matter, K.; Balda, M. S. ZO-1 Controls Endothelial Adherens Junctions, Cell–Cell Tension, Angiogenesis, and Barrier Formation. *Journal of Cell Biology* **2015**, *208* (6), 821–838. https://doi.org/10.1083/jcb.201404140.
(44) Zeng, J.; Matsusaki, M. Analysis of Thickness and Roughness Effects of Artificial Basement Membranes on Endothelial Cell Functions. *ANAL. SCI.* **2021**, *37* (3), 491–495. https://doi.org/10.2116/analsci.20SCP10.
(45) Kim, D.; Eom, S.; Park, S. M.; Hong, H.; Kim, D. S. A Collagen Gel-Coated, Aligned Nanofiber Membrane for Enhanced Endothelial Barrier Function. *Sci Rep* **2019**, *9* (1), 14915. https://doi.org/10.1038/s41598-019-51560-8.

(46) Zhuang, Y.; Zhang, C.; Cheng, M.; Huang, J.; Liu, Q.; Yuan, G.; Lin, K.; Yu, H. Challenges and Strategies for in Situ Endothelialization and Long-Term Lumen Patency of Vascular Grafts. *Bioactive Materials* **2021**, *6* (6), 1791–1809. https://doi.org/10.1016/j.bioactmat.2020.11.028.

(47) Trappmann, B.; Baker, B. M.; Polacheck, W. J.; Choi, C. K.; Burdick, J. A.; Chen, C. S. Matrix Degradability Controls Multicellularity of 3D Cell Migration. *Nat Commun* **2017**, *8* (1), 371. https://doi.org/10.1038/s41467-017-00418-6.

(48) Kleinman, H. K.; Martin, G. R. Matrigel: Basement Membrane Matrix with Biological Activity. *Semin Cancer Biol* **2005**, *15* (5), 378–386. https://doi.org/10.1016/j.semcancer.2005.05.004.

(49) Montesano, R.; Vassalli, J. D.; Baird, A.; Guillemin, R.; Orci, L. Basic Fibroblast Growth Factor Induces Angiogenesis in Vitro. *Proc Natl Acad Sci U S A* **1986**, *83* (19), 7297–7301.

(50) Thomsen, M. S.; Routhe, L. J.; Moos, T. The Vascular Basement Membrane in the Healthy and Pathological Brain. *J Cereb Blood Flow Metab* **2017**, *37* (10), 3300–3317. https://doi.org/10.1177/0271678X17722436.

(51) Ryma, M.; Genç, H.; Nadernezhad, A.; Paulus, I.; Schneidereit, D.; Friedrich, O.; Andelovic, K.; Lyer, S.; Alexiou, C.; Cicha, I.; Groll, J. A Print-and-Fuse Strategy for Sacrificial Filaments Enables Biomimetically Structured Perfusable Microvascular Networks with Functional Endothelium Inside 3D Hydrogels. *Advanced Materials* **2022**, *34* (28), 2200653. https://doi.org/10.1002/adma.202200653.

(52) Hoshino, Y.; Haberaecker, W. W. I.; Kodama, T.; Zeng, Z.; Okahata, Y.; Shea, K. J. Affinity Purification of Multifunctional Polymer Nanoparticles. *J. Am. Chem. Soc.* **2010**, *132* (39), 13648–13650. https://doi.org/10.1021/ja1058982.

(53) Kadowaki, K.; Matsusaki, M.; Akashi, M. Control of Cell Surface and Functions by Layer-by-Layer Nanofilms. *Langmuir* **2010**, *26* (8), 5670–5678. https://doi.org/10.1021/la903738n.

(54) Deligöz, H.; Tieke, B. QCM-D Study of Layer-by-Layer Assembly of Polyelectrolyte Blend Films and Their Drug Loading-Release Behavior. *Colloids and Surfaces A: Physicochemical and Engineering Aspects* **2014**, *441*, 725–736. https://doi.org/10.1016/j.colsurfa.2013.10.033.

(55) Lvov, Y.; Ariga, K.; Ichinose, I.; Kunitake, T. Assembly of Multicomponent Protein Films by Means of Electrostatic Layer-by-Layer Adsorption. *J. Am. Chem. Soc.* **1995**, *117* (22), 6117–6123. https://doi.org/10.1021/ja00127a026.

(56) Boulanouar, O.; Fromm, M.; Bass, A. D.; Cloutier, P.; Sanche, L. Absolute Cross Section for Loss of Supercoiled Topology Induced by 10 eV Electrons in Highly Uniform /DNA/1,3-Diaminopropane Films Deposited on Highly Ordered Pyrolitic Graphite. *The Journal of Chemical Physics* **2013**, *139* (5), 055104. https://doi.org/10.1063/1.4817323.

(57) Ton-That, C.; Shard, A. G.; Bradley, R. H. Thickness of Spin-Cast Polymer Thin Films Determined by Angle-Resolved XPS and AFM Tip-Scratch Methods. *Langmuir* **2000**, *16* (5), 2281–2284. https://doi.org/10.1021/la990605c.

(58) Boulanouar, O.; Khatyr, A.; Herlem, G.; Palmino, F.; Sanche, L.; Fromm, M. Soft Adsorption of Densely Packed Layers of DNA-Plasmid·1,3-Diaminopropane Complexes onto Highly Oriented Pyrolitic Graphite Designed To Erode in Water. *J. Phys. Chem. C* **2011**, *115* (43), 21291–21298. https://doi.org/10.1021/jp207083r.

(59) *Measuring surface zeta potential using phase analysis light scattering in a simple dip cell arrangement | Elsevier Enhanced Reader*. https://doi.org/10.1016/j.colsurfa.2011.12.065.

(60) Vasconcelos, J. M.; Zen, F.; Stamatin, S. N.; Behan, J. A.; Colavita, P. E. Determination of Surface ζ-Potential and Isoelectric Point of Carbon Surfaces Using Tracer Particle Suspensions. *Surface and Interface Analysis* **2017**, *49* (8), 781–787. https://doi.org/10.1002/sia.6223.

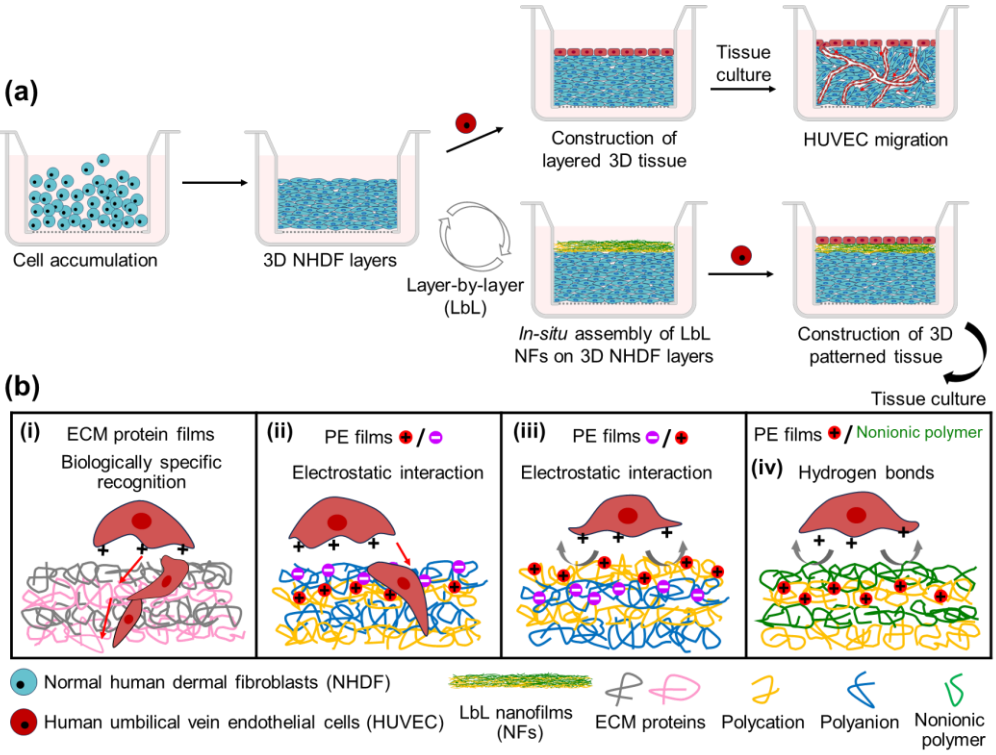

Scheme 1. (a) Schematic representation of the development of A-BMs by in situ LbL assembly technology on fibroblast tissues to construct 3D organized biological tissues composed of NHDF and HUVEC. In the absence of A-BMs, HUVEC migrate during tissue culture, thereby altering the 3D hierarchical tissue structure. (b) Comparison of the barrier function of various types of LbL films assembled from different ECM proteins and polymers to inhibit HUVEC migration during tissue culture.

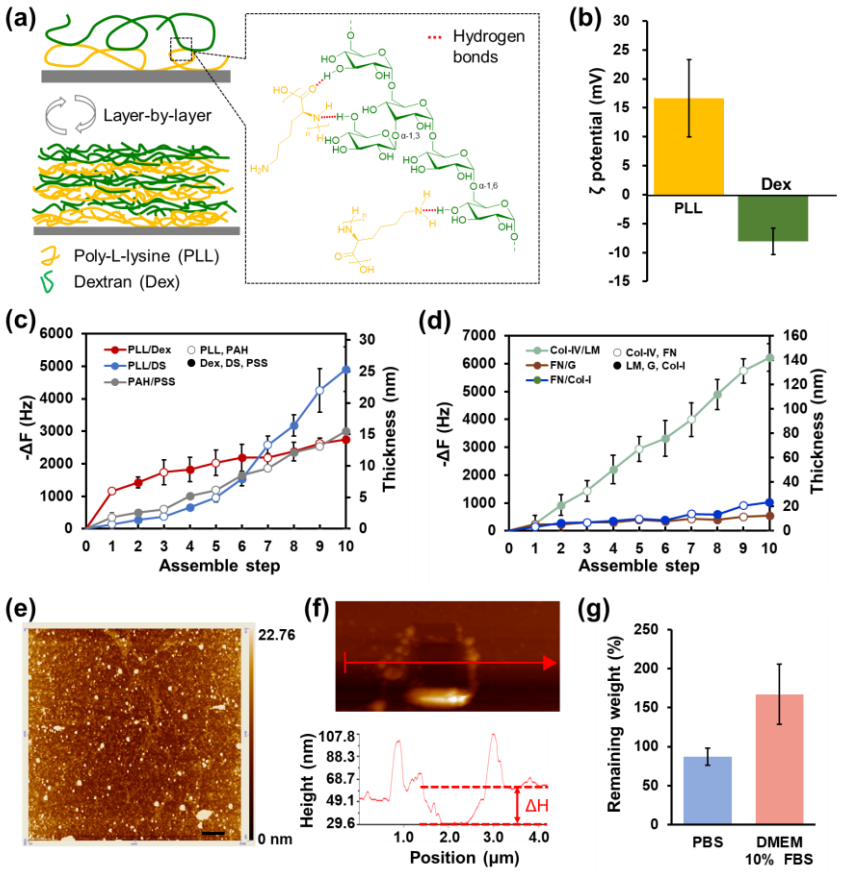

Figure 1. **Buildup of PLL/Dex multilayered ultrathin nanofilms (NFs) on QCM chips.** (a) Schematic illustration of the LbL assembly process of PLL and Dex via hydrogen bonds. (b) ζ potential of PLL (0.1 wt%) and Dex (0.1 wt%)/Tris-HCl buffer solutions (50mM, pH=7.4, 37 °C). n=3. (c) & (d) Frequency shifts and film thickness increases during assembly are summarized for various LbL films composed of polymers or ECM proteins. Frequency changes were recorded by QCM during assembly in 50 mM Tris-HCl buffer solution (pH=7.4, 37 °C). The concentration of each polymer or protein is 0.1wt%. (e) AFM tapping mode image (10 × 10 μm) of multilayers composed of PLL and Dex. Scale bar: 1 μm. (f) Scratching with the AFM tip creates a square hole of the PLL/Dex NFs, where the depth ΔH corresponds to the film thickness. (g) The remaining weight percentage of PLL/Dex NFs after immersion in PBS and DMEM/10% FBS for 60 min at 37 °C, which is summaried from the frequency change recoarding by QCM.

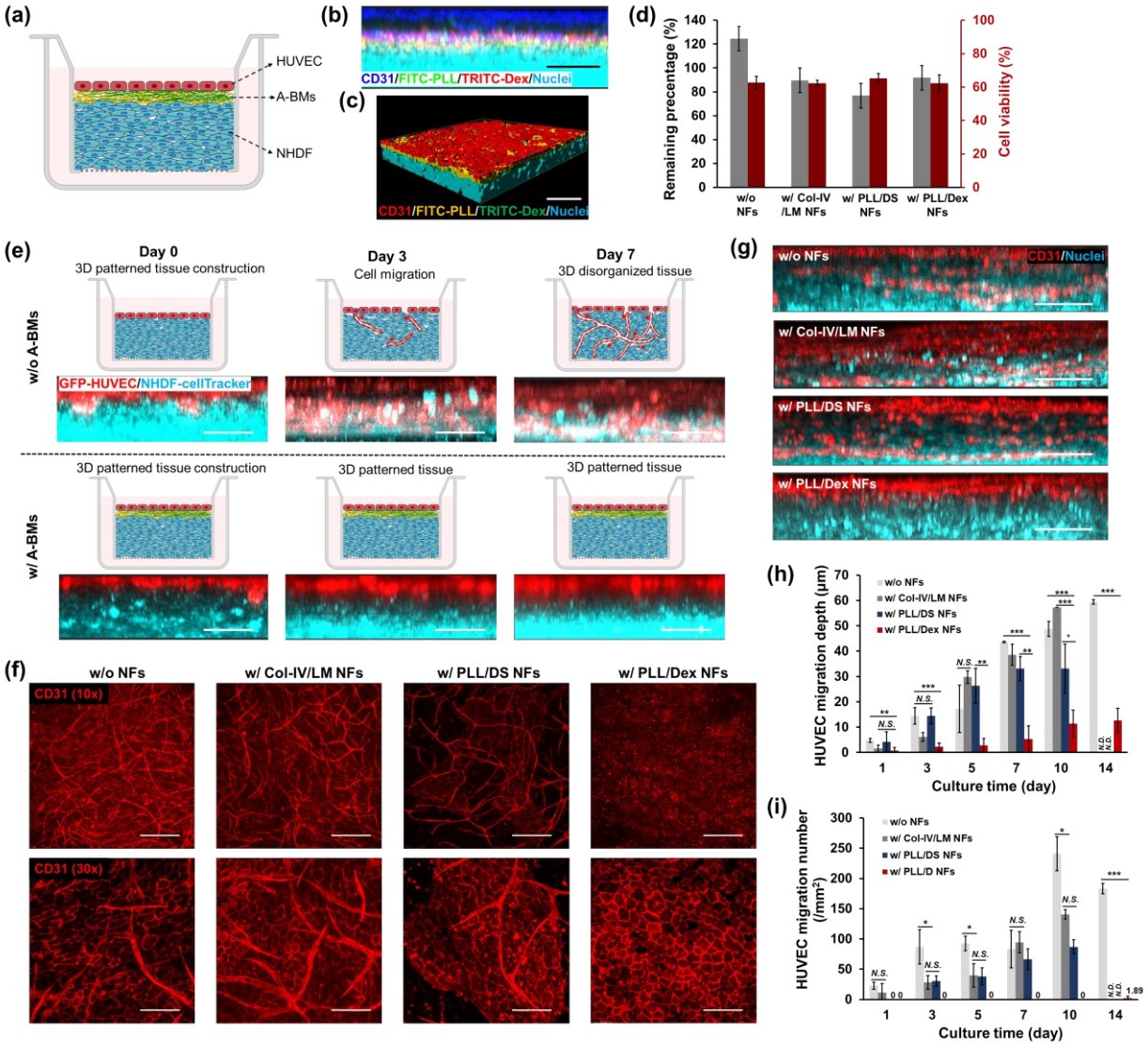

Figure 2. Barrier function of multilayered nanofilms on the compartmentalized co-culture of NHDF and HUVEC. (a) Schematic representation of the constructed 3D patterned tissue structure composed of HUVEC, A-BMs and NHDF, respectively. (b) Cross-sectional CLSM image showing the location of PLL/Dex NFs (FITC conjugated PLL in green and TRITC conjugated Dex in red) between the HUVEC monolayer (immunostained for CD31 in blue) and NHDF layers (stained with Hoechst 33342 in cyan). Scale bar: 50 μm. (c) 3D reconstructed CLSM image of compartmentalized cell co-culture system. Scale bar: 100 μm. (d) Cell number counting (gray and left) and cell viability (red and right) of NHDF layers after *in-situ* LbL assembly treatment and then cultured overnight. n=3. (e) up: Schematic representation of the structure of 3D patterned tissue during 7 days of culture. In the absence of any physical barrier, HUVEC gradually

migrate towards the fibroblast tissues, thereby altering their organized structure. With the support of A-BMs, the 3D organized tissue structure is preserved by inhibiting the migration of HUVECs. bottom: Cross-senctional CLSM images are displayed the changes in the relative positions of NHDF and HUVEC during the tissue culture. HUVEC are labeled with GFP (shown in red) and NHDF are stained with cellTracker deep red (shown in cyan). Scale bar: 50 μm. (f) Immunostaining of HUVEC with CD31 visualized by CLSM. The 3D scanning results of the co-culture system, from top to bottom, are compressed to single image. up: observed with 10× magnification, scale bar: 300 μm. bottom: observed with 30× magnification, scale bar: 100 μm. (g) Cross-sectional CLSM images of co-culture system with different LbL films observed after 7 days of culture. HUVEC are stained with CD31 shown in red and all cell nuclei are stained with Hoechst 33342 in cyan to show the position of NHDF. Scale bar: 50 μm. (h) HUVEC migration depth (compared with the position of HUVEC at Day 0) and (i) number of migrated HUVEC towards NHDF layers during the co-culture with different LbL films for 14 days. (h) n=3, (i) n=6. *p<0.05, **p<0.01, ***p<0.001. *N.S.* no significant difference. *N.D.* no data.

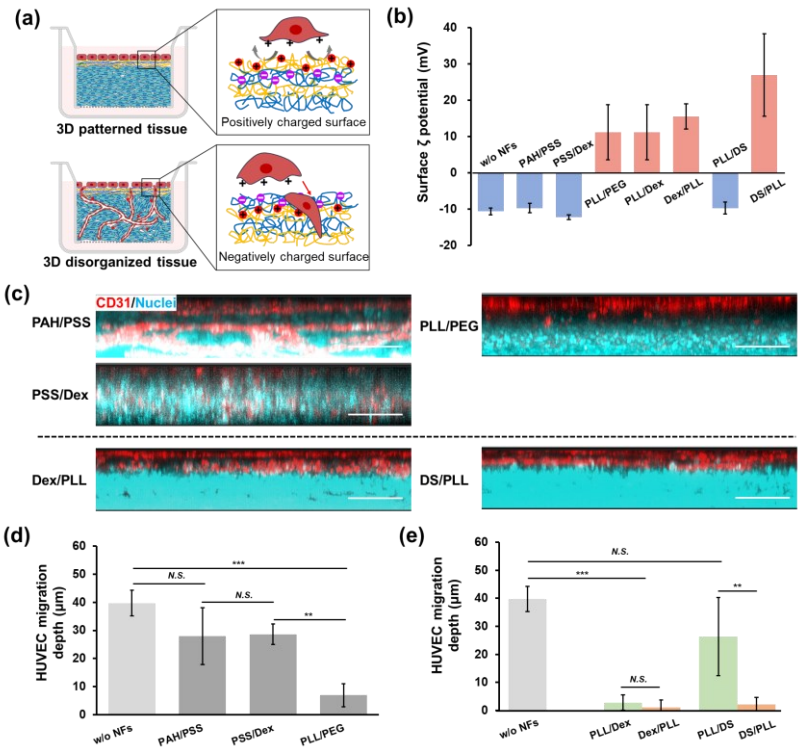

Figure 3. Effects of film outmost surface charge on HUVEC migration. (a) Schematic illustration depicts the correlations between the barrier functions of LbL films in preventing cell migration and preversing the organized tissue structure and their out most surface charge. (b) Surface ζ potential of various polyelectrolyte multilayered nanofilms assembled on a glass substrate in 50 mM Tris-HCl buffer solution (pH 7.4) at 37 °C. The measurement of ζ potential is performed in the same buffer solutions suspend with Nile Red-polystyrene nanoparticles as tracer particles (0.0005 wt%) at room temperature. n=3. (c) Cross-sectional CLSM images of co-culture system with various LbL films, which are observed after 7 days of culture. Scale bar: 50 μm. (d) and (e) HUVEC migration depth through various LbL NFs after 7 days of co-culture. n=3, $^{**}p<0.01$, $^{***}p<0.001$. *N.S.* no significant difference.

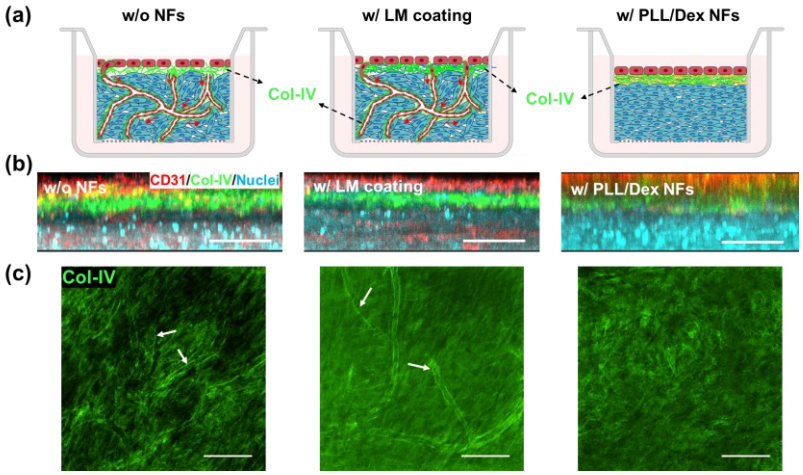

Figure 4. **Regeneration of natural BMs in 3D tissues.** (a) Schematic illustration of the assembly and position of Col-IV that is the main compoents of natural BMs between different cells in the co-culture system. (c) Relative position of Col-IV between HUVEC manolayer and NHDF layers after 7 days of culture. HUVEC is marked by CD31 in red, Col-IV is immunofluorescent stained in green, and nuclei are stained with Hoechst 33342 in cyan to show the location of NHDF. Scale bar: 50 μm. (c) Immunofluorescent staining of Col-IV in 3D tissues. White arrows indicate the assembly of secreted Col-IV along the capillary wall, where the capillary network is formed due to the migration of HUVEC into the fibroblast tissue. Scale bar: 300 μm.

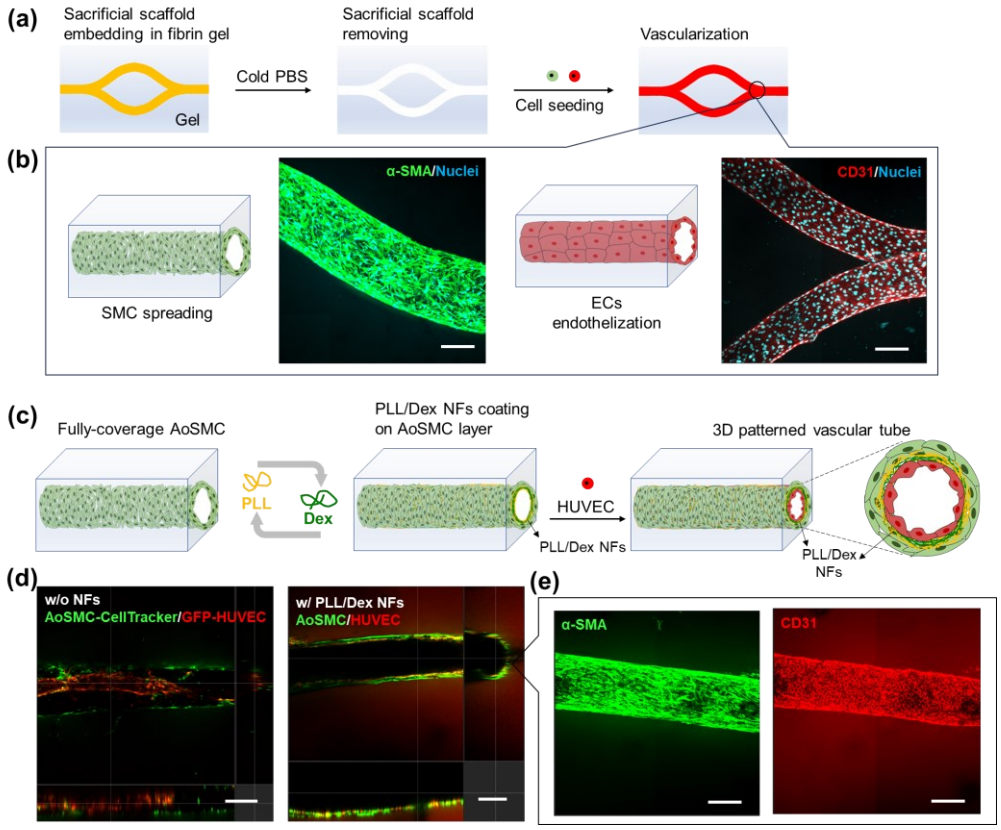

Figure 5. **Fabrication of 3D patterned vascular structure.** (a) Schematic illustration of cells seeded within microchannels in fibrin gels that were formed by sacrificial scaffold fixation and scaffold dissolution washing with cold PBS. (b) Schematic and CLSM images of the α-SMA positive AoSMC layer and CD31 positive HUVEC monolayer in microchannels. Nuclei are stained with Hoechst 33342. Scale bar: 200 μm. (c) Schematic reprentation of the *in-situ* LbL assembly of PLL/Dex NFs on AoSMC layers in the microchannels, and the construction 3D patterned vascular tube composed of AoSMC layers and a HUVEC monolayer, facilitated by the support of PLL/Dex NFs between the cells. (d) Orthogonal views (xy, xz, and yz) of the CLSM images illustrate the colocalization of AoSMC and HUVEC after culture for 5 days. Left: without PLL/Dex NFs, GFP-HUVEC detach from AoSMC layer (labeled with cellTracker deep red) and aggregate, blooking the microchannel. Right: with the assistance of PLL/Dex NFs, confluent HUVEC monolayer (makerked with CD31) is surround by compartmentalized AoSMC (stained with α-SMA). Scale bar: 200 μm. (e) Top-view of CLSM images demonstrate the morphology of the spreading AoSMC layers and the confluent HUVEC monolayer in the 3D patterned vascular tube. Scale bar: 200 μm.